Rogue Lateral Buckle Initiation at Subsea Pipelines

Navid Vosooghi, Ana Ivanović*, Srinivas Sriramula

School of Engineering, University of Aberdeen, Aberdeen, United Kingdom
*Corresponding author: a.ivanovic@abdn.ac.uk

ABSTRACT

Due to the pipelay vessel motions during installation of a subsea pipeline, as-laid direction of the pipeline changes along a nominally straight section of the route. In a High Pressure High Temperature (HPHT) pipeline, presence of rogue lateral Out of Straightness (OoS) can adversely influence the reliability of buckle initiation at engineered buckling sites e.g. sleepers. This implies the requirement to study the rogue buckle initiation to ensure unwanted buckles are not formed. This paper provides a framework to study the range of critical buckling force (CBF) of a rogue OoS which, so far has not been fully explored in the literature. A simplified and yet accurate pipe-soil interaction model for sandy seabeds, suitable for calculation of CBF is described. The built-in friction models in Abaqus FE software are not suitable for simulation of the lateral buckling as they cannot decouple axial and lateral force-displacement relationships. Therefore, a novel Finite Element (FE) modelling technique benefiting from a two-surface seabed capable of decoupling contact frictions at orthogonal directions is developed. This eliminates the need for developing complex user-defined friction subroutines. Different ways of characterising rogue lateral OoS are discussed and the best method is selected. Accordingly, and in a systematic process, pipe-soil interaction parameters, lateral OoS configuration parameters and pipeline stiffness which form the contributing parameters to the resistance against lateral buckling are identified.

Keywords: Subsea Pipeline, Lateral Buckling, Rogue Lateral OoS and buckle initiation.

1. INTRODUCTION

A key challenge in a pipeline lateral buckling design concept, where the presence of controlled buckles at deliberate locations is allowed, is to ensure that the buckles are initiated and formed at the expected locations. There are various methods such as use of sleepers, snake lay, buoyancy modules and residual curvature to initiate the buckles along the pipeline route [1]. In general, each of those methods introduce a combination of an Out of Straightness (OoS) and /or reduction in soil lateral resistance to trigger buckles at a low driving force. However, it is likely that the rogue lateral OoS, which are caused by pipelay vessel motions during pipeline installation, trigger unwanted buckles at a

lower driving force. The unwanted rogue buckles may experience excessive bending curvature causing local buckling which is considered as a failure mode [2] and therefore, deemed as not acceptable. There have been numerous cases where buckle initiators failed to either trigger buckles or lateral buckles were formed at unexpected locations [3,4]. This implies that the design of a buckle initiator shall ensure that the pipeline critical buckling force (CBF) at the initiator is lower than the adjacent rogue lateral OoS locations. This is a challenging task as it involves defining contributing parameters and their range, characterising the shape of the rogue lateral OoS and developing a suitable finite element modelling technique.

Hobbs et al [5,6] developed the differential equation of a laterally deflected pipeline by treating the pipeline as a beam-column which could be used to determine the CBF. However, it assumed that the pipeline was initially straight and therefore, not suitable for cases where the pipeline contains an initial imperfection. Taylor et al [7] advanced Hobbs' studies and derived an expression relating the length and maximum deflection of the initial imperfection, assuming that the shape of the initial imperfection follows the equation of a deflected pipeline. As the shape of a rogue OoS (acting as initial imperfection) does not follow this assumption, Taylor's analytical solution would not be suitable for rogue lateral OoS. Maltby et al. [8,9] presented a simplified solution to calculate the CBF of a pipeline with sinusoidal initial imperfection based on classical beam-column differential equation. However, the applied boundary conditions were not reflective of pipeline condition at the ends of an imperfection. This implies the requirement to utilise Finite Element (FE) modelling for computing the CBF of a pipeline with an initial imperfection. The built-in friction models in Abaqus FE software are not suitable for simulation of lateral buckling as they cannot decouple axial and lateral force-displacement relationships. Therefore, Abaqus FRIC subroutine needs to be utilised to decouple contact frictions and to describe the transmission of shear forces between surfaces [10,11]. Use of subroutines is a technically complex task and computationally expensive solution as it slows down the FE simulation [12,13,14]. This suggests the need to develop a simplified technique to use built-in friction models in Abaqus.

Researchers including Rathbone et al [15], constructed the shape of a rogue lateral OoS (i.e. as-laid geometry) based on the worse manoeuvring that a laybarge needs to take to correct the lay route. However, this solution is not suitable for a generic and parametric study as it is computationally expensive requiring modelling of the full pipelay process and therefore, will not be further studied in this research. There are approaches to define a geometrical configuration of OoS with a certain value of maximum curvature which are studied in this paper. Rathbone et al [16] suggest an offset configuration by using a small arc to connect two segments of the straight pipes.

Generally pipe-soil interaction is simplified by utilising force-displacement relationships [17,18,19]. Palmer et al [20] and Verley et al [21] provide guidelines to define the relevant frication values and associated mobilisations.

It is therefore important for pipeline engineers to develop a detailed and yet simple framework for obtaining the range of CBF of a rogue lateral OoS, as the available studies in the public domain do not

cover all the relevant aspects. In this paper, generic force-displacement relationships representing pipe-soil interaction on sandy seabeds are simplified to capture lateral buckle initiation. The numerical values of parameters defining pipe-soil interaction are derived based on recent recommendations of DNVGL-RP-F114 [22] which incorporate SAFEBUCK JIP guidelines. Single, double sinusoidal and combined sinusoidal-circular construction methods of the lateral OoS are studied and the most appropriate method selected and, subsequently, lateral OoS configuration is characterised. To avoid the complex task of developing subroutines, a novel FE modelling technique using the built-in Abaqus anisotropic friction model is developed. The contributing parameters towards the CBF and their range are defined in a structured process. This provides a comprehensive framework to calculate the range of CBF of a rogue lateral OoS in a pipeline. Finally, the use of the framework proposed here is explained by means of a numerical example.

2. PIPE- SOIL INTERACTION

An appropriate modelling of the soil surrounding the pipeline and seabed surface deformation due to the lateral and axial movements of the pipeline requires large strain finite element analysis [23,24] with progressive re-meshing which makes this task impractical for engineering applications. Instead, the forces imposed on the pipeline by the seabed at various stages of the pipeline axial and lateral movements can be represented and applied as force-displacement relationships [17]. There is limited research within the public domain addressing pipeline large lateral displacement on sandy seabeds. Palmer et al [20] presented the results of a Joint Industry Partnership (JIP) led by Danish Hydraulic Institute (DHI) on stability of the pipelines on sandy seabed involving large displacements. A more recent work by Verley et al [21] shows the development of a pipe-soil interaction model for sandy soils which could predict the pipe embedment and lateral resistance at various stages of the lateral movement i.e. break-out and residual displacement. The axial and lateral soil resistance models which are used in this study are adapted from [22].

Soil Axial Resistance

The drained or undrained soil behaviour can be observed during pipeline axial movement depending on the rate of movement and soil characteristics [22]. For sandy soils studied here drained conditions apply, and the soil axial resistance presents a ductile behaviour with no peak [18,19]. However, for engineering purposes, a bi-linear force-displacement dependency (a tangent fit to the soil axial resistance curve) can be utilised (Figure 1). In a bi-linear model, soil resistance reaches its maximum at a mobilisation displacement ($\mathrm{Mob_{Ax}}$) and remains constant beyond that point. This behaviour is analogous to an elastic-perfectly plastic material model. The solid line in Figure 1 is used in this paper as the constitutive relationship in axial direction.

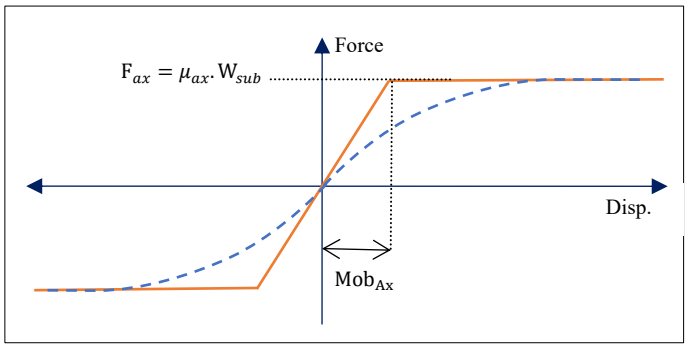

Figure 1. Soil Axial Resistance Model (Constitutive Relationship)

The soil interface friction coefficient (μ_{ax}) and axial resistance (F_{ax}) can be presented, according to [22], as:

$$\mu_{ax} = r_{pipe-sil}.tan\varphi\ .\zeta \quad (1)$$

$$F_{ax} = \mu_{ax}.W_{sub} \quad (2)$$

where W_{sub} is pipe submerged weight, $r_{pipe-sil}$ the pipe-soil roughness factor, φ friction angle of the soil and ζ wedging factor [25].

The low, best and high estimate values (LE, BE, HE) of the displacement at transition point of the bi-linear soil axial resistance (solid curve in Figure 1) are stated below [22]:

$$Mob_{ax-LE} = Min(1.25mm\ and\ 0.0025D) \quad (3)$$

$$Mob_{ax-BE} = Min(5mm\ and\ 0.01D) \quad (4)$$

$$Mob_{ax-HE} = Max(250mm\ and\ 0.5D) \quad (5)$$

Soil Lateral Resistance

Pipeline initial embedment takes place at installation phase due to the pipeline self-weight and static and dynamic installation loads. In the first stage of the lateral movement, pipeline breaks out from its partially embedded condition which is accompanied by the resistance of the berms (soil heave caused by pipe penetration into the seabed). Soil resistance is built up in this stage and gets to its maximum (shown as "a" in Figure 2) as the pipeline need to push the berm. The soil resistance and pipeline lateral displacement at this point are defined as F_{lat} and Mob_{lat}, respectively. The second stage (shown as "b" in Figure 2) is associated with large amplitude displacement [26] and as the pipeline has crossed over the berm, soil resistance decreases and stabilises to a constant level called residual resistance. The soil resistance and pipeline lateral displacement at this point are defined as F_{lat_res} and Mob_{lat_res}, respectively. In view of the above, a tri-linear force-displacement relationship can represent

the soil resistance as outlined in Figure 2 (dotted line). The pipeline buckling is initiated and formed at the first and second stages, respectively.

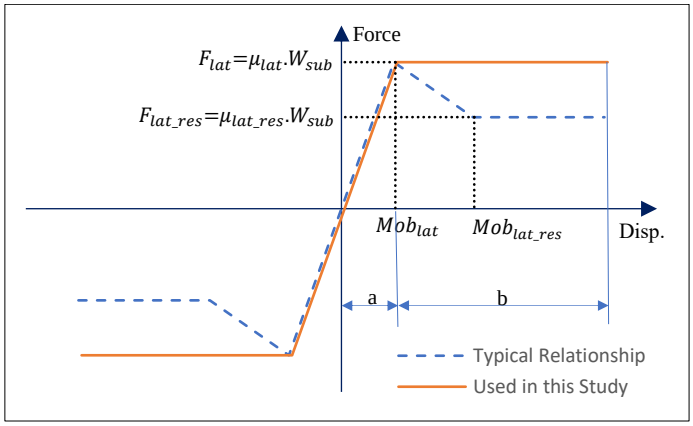

Figure 2. Soil Lateral Resistance Model (Constitutive Relationship)

The pipeline equivalent peak lateral friction coefficient (μ_{lat}) and peak lateral resistance (F_{lat}) can be presented, according to [22], as:

$$\mu_{lat} = 0.6 + \frac{\gamma D^2}{W_{sub}}.\left(5 - 0.15\frac{\gamma D^2}{W_{sub}}\right).\left(\frac{z}{D}\right)^{1.25} \quad (6)$$

$$\frac{z}{D} = 0.037\left(\frac{\gamma D^2}{W_{sub}}\right)^{-0.67} \quad (7)$$

$$F_{lat} = \mu_{lat}.W_{sub} \quad (8)$$

where D is the pipeline diameter, z pipeline embedment and γ soil submerged unit weight.

The low, best and high estimate values of the soil lateral peak mobilisation (Mob_{lat}) are stated below [22]:

$$Mob_{Lat-LE} = 0.004D + 0.02\left(\frac{z}{D}\right).D \quad (9)$$

$$Mob_{Lat-BE} = 0.02D + 0.25\left(\frac{z}{D}\right).D \quad (10)$$

$$Mob_{La-HE} = 0.1D + 0.7\left(\frac{z}{D}\right).D \quad (11)$$

In this study the initiation of the lateral buckles is of interest which happens as the pipeline passes the point: (Mob_{lat}, F_{lat}). Beyond this point, soil resistance decreases sharply and a lateral buckle is developed. Therefore, for a buckle initiation study, the initial part of the soil resistance model shown as "a" in Figure 2, is only relevant. In view of this, and to minimize modelling efforts, soil resistance beyond the peak value (F_{lat}) is assumed to remain constant and equal to the peak resistance. This results

in simplification of the soil resistance model to a bi-linear force-displacement relationship which is outlined as a solid curve in Figure 2. This can be represented as a Coulomb friction model and is used here as the constitutive relationship in lateral direction. It should be noted that the basic Coulomb friction model in which the frictional resistance increases linearly and then remains at its maximum value cannot accurately represent the pipe-soil interaction in a lateral buckling scenario where post-buckling behaviour of the pipeline (buckle development) is of interest.

3. PIPE-SOIL INTERACTION MODELLING TECHNIQUE

The constitutive relationships outlined in the previous section need to be captured in the FE model. This is not a simple task as pipe-soil interaction in axial and lateral directions are decoupled (independent) and have different values. The built-in capabilities of the Abaqus FE software package, used in this study, are not suitable for this task. Therefore, to overcome this challenge a new technique is required. In a general pipeline-seabed interaction problem, non-linear springs cannot be utilised as they are not automatically disengaged when pipeline-seabed contact does not exist (i.e. free spans) or is lost (i.e. initiation and development of a buckle on a sleeper). In addition, springs are defined based on global coordinate system and therefore, cannot follow the pipeline route or adjust their directions in a buckling scenario. This implies the requirement to utilise more advanced methods such as the frictional contact pressure-overclosure constitutive relationship.

The displacement of the pipeline at the location of lateral OoS is a combination of axial and lateral movements. Therefore, there is a need to use a friction model capable of capturing two different friction coefficients in the orthogonal directions on the contact surface coinciding with the slip directions (i.e. axial and lateral). In the classical isotropic Coulomb friction model, the shear stress between the contact surfaces can reach a certain value known as the critical shear stress, τ_{crit}, at which slip of the surfaces starts. The critical shear stress is the product of contact pressure, p, and coefficient of friction, μ, i.e. $\tau_{crit} = p.\mu$. The coefficient of friction is the same in all directions (isotropic friction). This implies that the isotropic Coulomb friction model is not representative as it cannot differentiate between orthogonal slip directions. The anisotropic friction model allows for different friction coefficients in orthogonal directions on the contact surface coinciding with slip directions. The critical shear surface is an ellipse as outlined in Figure 3 with $\tau_{crit\_ax} = W_{sub}.\mu_{ax}$ and $\tau_{crit\_lat} = W_{sub}.\mu_{lat}$, representing the extreme points of the axial and lateral stick/slip transition points, respectively.

This implies that if an anisotropic friction model is directly used, axial and lateral friction coefficients will be coupled. For example, if the combination of axial and lateral forces following the dotted line (Figure 3) are imposed, pipeline transits from stick state to slip state at Point-A. At this point, the components of combined stress (τ_{comb_ax} and τ_{comb_lat}) are smaller than the axial and / or

lateral critical shear stress. This clearly is not complying with the requirement of axial and lateral critical shear stresses being decoupled (independent). In addition, start of slip (pipeline movement) does not happen at the axial / lateral critical shear stress.

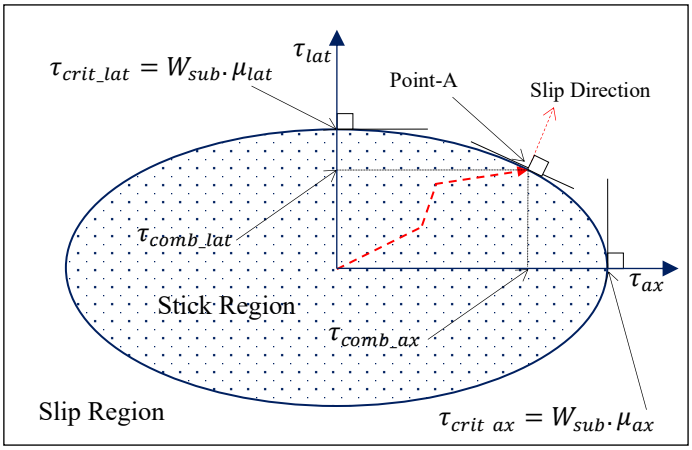

Figure 3. Critical Shear Stress Surface for the Anisotropic Fiction Model

To overcome this challenge a technique based on utilising two contact surfaces to model the seabed is developed here. In this proposed technique, two surfaces are placed at the same elevation and both interact with the pipeline (Figure 4). However, the frictional contact properties of the surfaces are altered. For the first surface which represents the axial friction only, anisotropic friction values are set to (μ_{ax}, 0). Likewise, the anisotropic friction of the second surface is set to (0, μ_{lat}) to represent lateral friction only. In this way, the axial displacements are captured by the first surface without imposing any resistance on the lateral displacements and in a similar way, second surface will react against lateral displacements only. As both surfaces are interacting with the pipeline, half of the pipeline weight is transferred to each of them. Consequently, axial and lateral friction coefficients should be multiplied by two to compensate for this. In this way axial and lateral friction values are decoupled and pipeline axial and lateral transition to slip state happens at $\tau_{crit\_ax} = \frac{W_{sub}}{2}.(\mu_{ax}.2)$ and $\tau_{crit\_lat} = \frac{W_{sub}}{2}.(\mu_{lat}.2)$, respectively. The seabed vertical stiffness ($Stiffness_{ver}$) needs to be halved as two surfaces are providing vertical resistance. To include axial and lateral mobilisations (see Figure 1 and Figure 2) an elastic slip needs to be introduced in the friction model. The elastic slip is based on a penalty method that permits some relative motion of the surfaces when they should be sticking. Abaqus calculates the elastic slip based on the average friction coefficient, $\bar{\mu}$, and average critical shear stress, $\overline{\tau_{crit}}$, [10, 11]. In the context of axial anisotropic friction surface defined above (μ_ax,0), following expressions can be derived:

$$\bar{\mu} = \sqrt{0.5((\mu_{ax}.2)^2 + 0^2)} \quad (12)$$

$$\overline{\tau_{crit\_ax}} = \bar{\mu}.\frac{W_{sub}}{2} = \frac{\sqrt{2}}{2}.\mu_{ax}.W_{sub} \quad (13)$$

Therefore, the mobilisation at which the axial slip happens is $\frac{\sqrt{2}}{2}$ of $\mu_{ax}.W_{sub}$. This needs to be compensated by multiplying the expected axial mobilisation by 2. The same applies to the lateral direction.

Based on the above, it can be concluded that a two-surface seabed can be utilised to correctly capture and decouple the pipeline-seabed axial and lateral displacement-force relationships. However axial and lateral frictions and mobilisations need to be altered as below before being used in the Abaqus anisotropic friction model:

$$\mu_{ax\_abaqus} = 2.\mu_{ax} \quad (14)$$

$$\mu_{lat\_abaqus} = 2.\mu_{lat} \quad (15)$$

$$Mob_{ax\_abaqus} = \sqrt{2}.Mob_{ax} \quad (16)$$

$$Mob_{lat\_abaqus} = \sqrt{2}.Mob_{lat} \quad (17)$$

$$Stiffness_{ver\_abaqus} = 0.5\ .Stiffness_{ver} \quad (18)$$

The two surfaces are modelled by using analytical rigid surface option rather than element-based option which eliminates the need for meshing. In addition, there is no requirement to define the width of the surface as the analytical surface is produced by infinite extrusion of its cross-section (which in case of a flat seabed is a straight line). This implies that both surfaces stated above have the same dimensions. The use of analytical rigid surface for contact problems is very beneficial as it decreases the time spent in contact tracking operation and will consequently decrease the computational cost significantly. In addition, it helps to reduce the contact noise [33]. The properties of the surface behaviour, which are assigned in the contact definition, are used to define the vertical and tangential stiffnesses to be translated into the pipeline vertical embedment in the seabed and the resistance of seabed against pipeline axial and lateral movements. An Abaqus input block defining the contact in lateral direction is included below. The values of "Stiffness_ver_abaqus", "Mob_lat_abaqus" and "Mu_lat_abaqus" are defined by Eq.18, Eq.17 and Eq. 15, respectively. Further details of the FE modelling can be obtained by contacting the authors.

```
*CONTACT PAIR, INTERACTION=SEABED_PIPE_LATERAL, TYPE=NODE TO SURFACE
PIPE_SURFACE, SEABED_SURF_LAT
*SURFACE INTERACTION, NAME=SEABED_PIPE_LATERAL
*SURFACE BEHAVIOR, PRESSURE-OVERCLOSURE=LINEAR
Stiffness_ver_abaqus
*FRICTION, ANISOTROPIC, ELASTIC SLIP=Mob_lat_abaqus
0, Mu_lat_abaqus
```

In order to validate the proposed modelling technique and to demonstrate that its results are in compliance with expected analytical values, the pipeline-seabed interaction of a straight section of a 10" (0.273m) dia, 18.2mm thick pipeline with a weight of 800 N/m is studied. A set of typical values

of μ_{ax}, μ_{lat}, Mob_{ax} and Mob_{lat} are used in this case and assumed to be 0.5, 0.8, 0.7m and 0.3m, respectively. A screenshot of the Abaqus model is shown in Figure 4.

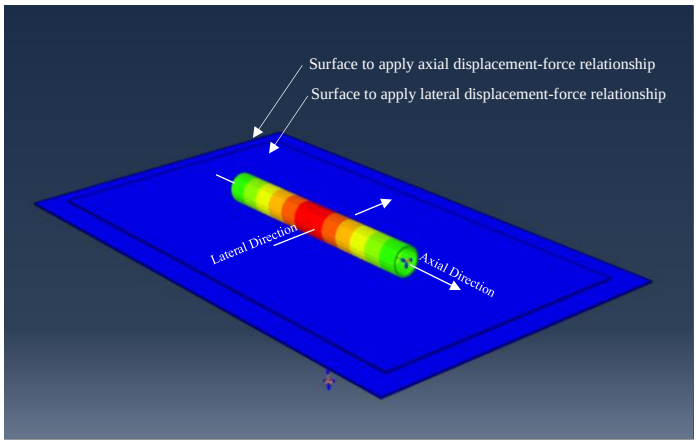

Figure 4. Abaqus Screenshot – Two Surface Contact Technique

Axial and lateral forces were imposed on the pipeline in a sequence to simulate the cases where axial force only, lateral force only or combined axial and lateral forces are developed during a lateral buckling scenario. Time history of the imposed loads are presented in Figure 5.

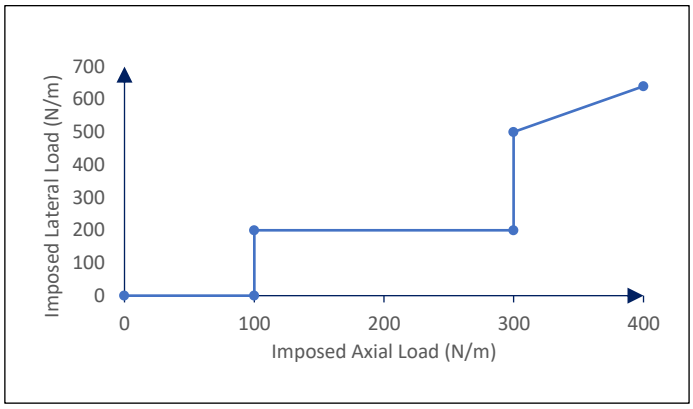

Figure 5. Time History of Axial and Lateral imposed Loads

At each step of the loading, axial and lateral displacements were extracted from Abaqus and compared with the expected analytical values. Imposed loads and displacements show less than 0.01% error in results (Table 1). In a specific direction (e.g. axial) and within the mobilisation distance, the analytical displacement is the ratio of applied load and soil peak resistance multiplied by the mobilisation value.

Step	Imposed Load (N)		Axial Displacement (mm)			Lateral Displacement (mm)		
	Axial	Lateral	Analytical	Abaqus	Error (%)	Analytical	Abaqus	Error (%)
1	100		175	174.99	<0.01			
2		200				93.75	93.74	<0.01
3	300	0	525	524.99	<0.01			
4		500				234.37	234.37	<0.01
5	400	640	700	699.99	<0.01	300	299.99	<0.01

Table 1. Comparison between FE and Analytical Results

Therefore, it can be concluded that the proposed FE modelling technique is validated for the purpose of this study and can successfully capture the expected constitutive relationships (solid lines in Figure 1 and Figure 2) in both axial and lateral directions.

To compare the errors due to direct use of Abaqus built-in anisotropic friction model, the same pipeline but with the value of 0.2m for both Mob_{ax} and Mob_{lat} is studied (built-in anisotropic model can accept one mobilisation value only). The elliptical critical shear surface for this example has radii of 400 N (800 N x 0.5) and 640 N (800 N x 0.8). Therefore, a combined loading of 200 N/m and 554.25 N/m in axial and lateral directions results in pipeline being exactly at transition from stick to slip state (Point-A in Figure 3). This can be confirmed by the FE model as any increase in loading results in entering into the slip region and as a consequence, FE simulation would not converge. The same pipeline is simulated in Abaqus but by utilising the modelling technique proposed above. The obtained displacements of both models are presented in Table 2 which shows a considerable difference between the results. The displacements from the proposed modelling technique are lower than mobilisation distance (20mm) and therefore, the pipeline is not entering into the slip region. This implies that the use of Abaqus built-in anisotropic friction model can introduce considerable errors in displacement values and slip / stick state.

Imposed Load (N)		Axial Displacement (mm)			Lateral Displacement (mm)		
Axial	Lateral	Proposed Technique	Abaqus Built-in Anisotropic	Error (%)	Proposed Technique	Abaqus Built-in Anisotropic	Error (%)
200	554.25	10	13.34	33.4	17.31	14.44	-16.58

Table 2. Comparison between Abaqus Built-in Friction Model and Proposed Technique

There are other phenomena such as extreme environmental conditions (wave and current) under which the loads are applied to the pipeline in arbitrary directions. The proposed modelling technique is also capable of capturing those conditions. In the decoupling process, each surface registers the pipeline force-displacement interaction in one direction only (e.g. axial) without getting any influence from other direction (e.g. lateral). This is due to the way anisotropic friction values of each surface are set. The friction coefficient value in the direction which is required to decouple from is set to zero i.e. (μ_ax, 0). For the cases where the pipeline experiences a combined loading in axial and lateral directions, the loading in each interval is decomposed to its components in axial and lateral directions. Then, the displacement in each direction is computed based on the tangential contact properties defined for the surface of that specific direction. Therefore, the resultant displacement, which is the vector summation of the displacements in orthogonal directions, corresponds to the original decomposed loading.

4. CONFIGURATION OF ROGUE LATERAL OOS

Post-lay survey data from nominally straight sections of the pipelines show that the pipeline local and global heading (as-laid direction) change along the route and the pipeline deviates by several meters from its expected straight nominal route [16]. A lateral OoS can be constructed by defining a geometrical configuration with a certain value of maximum curvature. To do this, the configuration of the OoS needs to be characterised and the dependency between the parameters defining its shape established.

Methods to Construct a Lateral OoS Configuration

In its simplest form, a rogue lateral OoS can be constructed by using a small arc (e.g. <100m) to connect two segments of the straight pipes in the middle [16]. In this method, three parameters i.e. arc length (L_{Arc}), bend radius (R) and offset angle (ϕ) characterise the geometry of the as-laid OoS. These parameters are related by:

$$L_{Arc} = R.\phi \tag{19}$$

Another approach is to utilise a sinusoidal wave shape to define the configuration of the pipeline at a lateral OoS:

$$f(x) = A.sin(Bx) + D \tag{20}$$

where A is the wave amplitude, $\frac{2\pi}{B}$ is the wavelength (i.e. $L = \frac{2\pi}{B}$) and D is the vertical shift (Figure 6).

A section of the sinusoidal curve between $\left(\frac{2n+1}{2B}\right)\pi$ and $\left(\frac{2n+5}{2B}\right)\pi$ is more of interest as it results in having a lateral OoS with one crown on one side of the pipeline which can easily be used to assemble

several lateral OoS on the pipeline route. That section is labelled as "Single Sinusoidal Curve" in Figure 6. The maximum curvature (κ_{max}) of the sinusoidal curve which happens at $\left(\frac{2n+3}{2B}\right)\pi$ is equal to:

$$\kappa_{max} = AB^2 \tag{21}$$

By substituting wavelength equation into curvature equation, the following relationship, which connects wavelength (L), maximum curvature (κ_{max}) and amplitude (A) is obtained:

$$A = \frac{\kappa_{max}}{4\pi^2} L^2 \tag{22}$$

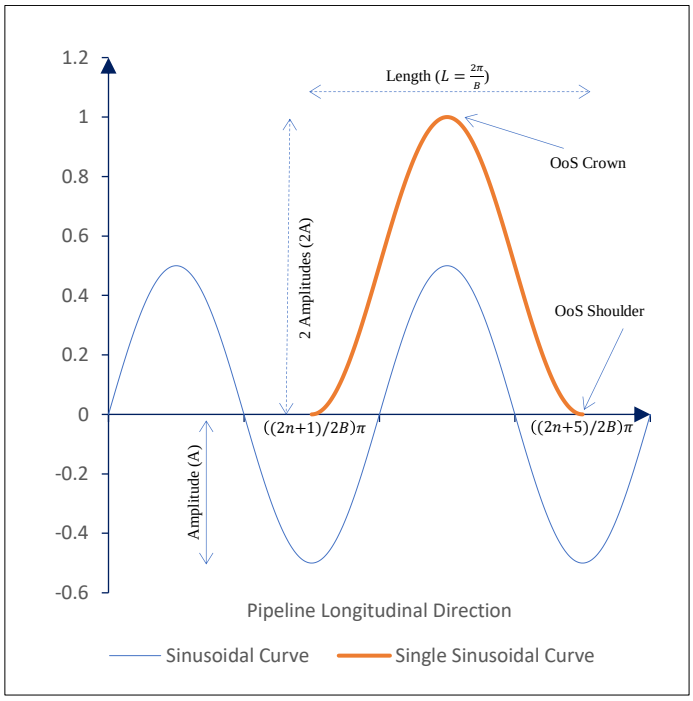

Figure 6. Single Sinusoidal Lateral OoS Configuration

The advantage of Eq. 22 is to define a sinusoidal OoS by two parameters i.e. maximum curvature and wavelength only. By substituting above equations into Eq. 22, a sinusoidal wave shape can be expressed as following:

$$f(x) = \frac{\kappa_{max}}{4\pi^2}.L^2.\left[1 + sin(\frac{2\pi}{L}.x)\right], \qquad \frac{1L}{4} \le x \le \frac{5L}{4} \tag{23}$$

To facilitate the formation of the buckle at the crown (rather than shoulders) two single sinusoidal waves were superimposed to form a double sinusoidal configuration (Figure 7). The main sinusoidal wave with the desired curvature and wavelength was constructed first. Then, a secondary sinusoidal

wave with a larger curvature was superimposed on the main curve so that they intersect at their inflection points. As the transition from the main to the secondary curve takes place at inflection points, $\left(\frac{n+1}{B}\right)\pi$ and $\left(\frac{n+2}{B}\right)\pi$, a smooth transition is experienced. This should promote buckle initiation at crown due to its greater curvature.

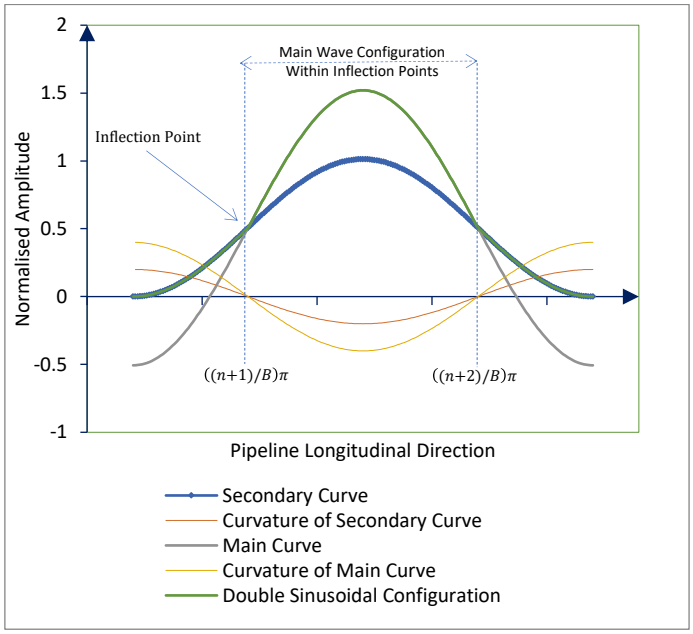

Figure 7. Double Sinusoidal Lateral OoS Configuration

Another possibility is to construct a combined curve by superimposing circular arcs with a larger curvature at the sides of a partial sinusoidal curve. In this context, a partial sinusoidal curve refers to a section of the curve which is between the inflection points. Each circular arc is placed in such way so that one end is tangential to the partial sinusoidal curve (at inflation points) and the other end is tangential to the straight route of the pipeline.

Selection of the Lateral OoS Construction Method

In offset angle configuration, two straight segments of the pipeline adjacent to the arc (lateral OoS) are not aligned. This makes this method unsuitable for assembling rogue lateral OoS on the pipeline route in the FE model. To assess the suitability of single, double, and combined sinusoidal configurations, several FE simulations were carried out by utilising the pipe-soil interaction constitutive relationships and the modelling technique explained in this paper. The results showed that if double or combined sinusoidal configurations were used, the buckles were initiated at transition points rather than at the crown. Therefore, it is concluded that the single sinusoidal configuration i.e. the curve labelled as “Single Sinusoidal Curve” in Figure 6, meets the expected buckling behaviour and therefore, will be used in this study.

5. CONTRIBUTING PARAMETERS IN BUCKLE INITIATION

In a lateral buckle initiation scenario, driving force builds up during pipeline start-up due to pressure and temperature increase to a point where resisting forces fail to provide any further resistance. At this point the buckling is initiated and pipeline undergoes large lateral displacements. The driving force i.e. effective axial force (S) is predominantly a function of pressure, temperature and pipe steel cross-sectional area [27]:

$$\boldsymbol{S = -\Delta P_i A_i (1 - 2\upsilon) - A_s E \alpha \Delta T} \quad (24)$$

where ΔP_i is internal pressure increase, ν Poisson's ratio, A_s steel area, E Young's modulus, α coefficient of thermal expansion and ΔT temperature increase.

Buckling is resisted by the pipeline bending stiffness and soil lateral (and axial) resistance. The bending stiffness is a function of the pipeline moment of inertia ($\boldsymbol{I}$) which in turn, is a function of diameter and thickness. The soil lateral resistance ($\mathbf{F}_{\boldsymbol{lat}}$) is a function of the lateral friction coefficient ($\boldsymbol{\mu_{lat}}$), mobilisation displacement ($\mathbf{Mob}_{\boldsymbol{lat}}$) and pipeline submerged weight ($\mathbf{W}_{\boldsymbol{sub}}$) where, in turn the submerged weight is a function of the pipeline diameter, thickness and the density of the pipeline content ($\boldsymbol{\rho_{cont}}$). The soil axial resistance ($\mathbf{F}_{\boldsymbol{ax}}$) is a function of the axial friction coefficient ($\boldsymbol{\mu_{ax}}$), mobilisation displacement ($\mathbf{Mob}_{\mathbf{Ax}}$) and pipeline submerged weight. In addition, the pipeline CBF is particularly influenced by the level of the pipeline initial configuration (lateral OoS) which acts like a trigger i.e. more severe OoS result in a smaller buckling force. If pipeline initial configuration is idealised by a sinusoidal wavelength, it can be characterised by its wavelength ($\boldsymbol{L}$) and maximum curvature ($\boldsymbol{\kappa_{max}}$). Contributing parameters in the pipeline resistance against lateral buckling and their dependencies are outlined in Figure 8.

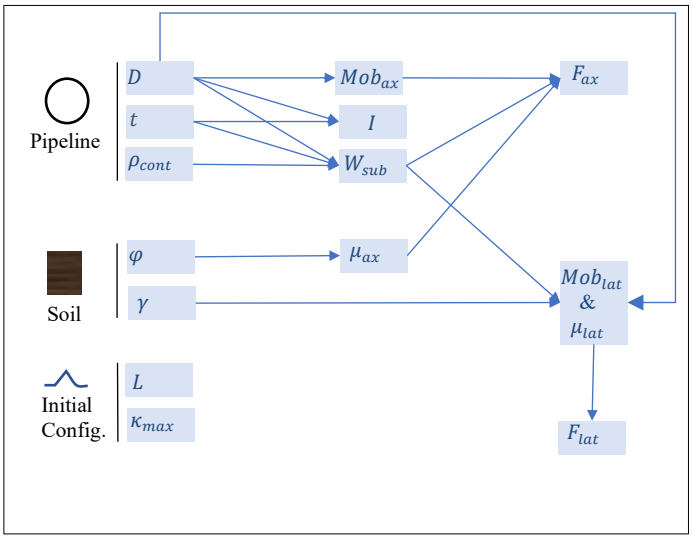

Figure 8. Contributing Parameters in Pipeline Critical Lateral Buckling (resistance)

The loading history, i.e. the sequence of pressure and temperature increase, in a specific pipeline does not influence the CBF. This can be because of the buckling capacity being dependent on the pipeline stiffness, boundary conditions, and initial imperfections only [28]. In view of this, loading history is a non-contributing parameter. The external pressure which is a function of the water depth does not influence the buckling force. During installation and in fully restrained sections of the pipeline, touchdown point can be considered as an axially fixed point. However, the adjacent point on catenary is free to move axially which results in release of the axial strain caused by hoop stress due to external pressure [28]. Consequently, external pressure/water depth is a non-contributing parameter. The effects of hydrodynamic loads (wave and current) induced by extreme environmental conditions can be included by normalising the pipeline lateral frication coefficient (μ_{lat_eq}) to incorporate the effects of the lift (F_L) and drag forces (F_D) as [34]:

$$\mu_{lat\_eq} = \frac{\mu_{lat}.(W_{sub}-F_L)-F_D}{W_{sub}} \quad (25)$$

The ocean wave-induced seabed liquefaction can severely affect the pipeline OoS and the soil resistance by introducing seabed instability. In sandy seabeds, wave cyclic loading may cause the soil to lose its shear strength resulting in transformation of the soil-water mixture under (or in the vicinity of) the pipeline into the liquid. Liquefaction can be categorised into instantaneous and residual. The former is caused by passage of the wave trough which causes excess pressure at a depth below the seabed surface. This results in the seepage of the flow in upward direction and pressure lift force which can lift a column of the soil [36]. The latter is caused by compacting effects of the waves on loosely deposited sediments creating an excess pore pressure in the seabed depending on the permeability of the soil and rate of the applied load [37]. If this pressure becomes sufficient, effective stress of the soil can disappear resulting in liquefaction.

Liquification can force the pipeline to move vertically and / or laterally provided: pipeline specific gravity is different from the liquified surrounding soil, and the liquefaction occurs simultaneously at a distance along the pipeline at which the pipeline stiffness is not sufficient to prevent the pipeline from movement [36]. Those movements introduce pipeline OoS which can trigger initiation and development of the unwanted buckles. However, as the subject of this paper is the buckling of pipelines due to the pressure and temperature effects, the adverse impacts of the seabed liquefaction are not studied any further. It is also worth mentioning that the pipelines within the diameter range studied in this paper are manly laid in the deep waters at which the environmental loads are minimal. In shallow waters, those pipelines are protected (buried) to avoid the interference with fishing / trawling activities and therefore, they are not subject to the lateral buckling.

6. RANGE OF PARAMETERS

Lateral buckling is mainly experienced by the High Pressure High Temperature (HPHT) production pipelines between subsea wells / manifolds and receiving facilities containing well fluids which are of high temperature and pressure. Typical diameter sizes of such pipelines are between 6" to 16" which is the range considered in this study. The pipeline thickness is predominantly a function of the internal and external pressures and therefore can vary over a wide range. Therefore, for each of the selected pipeline diameters stated above, the standard pipe thicknesses (t) are extracted from ASME B36.10M [29], while the thicknesses which result in positive pipeline submerged weight are selected as realistic thicknesses for that specific pipe diameter.

The range of parameters contributing to the pipeline-seabed interaction needs to be defined. The soil axial friction coefficient, Eq. (1), covers a wide range between 0.3 and 1 [22] and as such the whole range needs to be considered. The error bars are used in this paper to graphically represent the variability of data from a specific data point in terms of error percentage. The numerical values of the best estimate of soil axial mobilisation are calculated based on Eq. (4) and are plotted in Figure 9 covering a range between 1.68 mm to 4.06 mm. The error bars (vertical lines with end caps) with an error percent of 45 % are required to cover the whole range of values (horizontal solid lines). This high error percentage implies that a fixed value of axial force mobilisation cannot be used and therefore, the whole range of values needs to be studied. However, for a specific pipeline, by utilising Eq. (3) to Eq. (5), the range of axial mobilisation can be established.

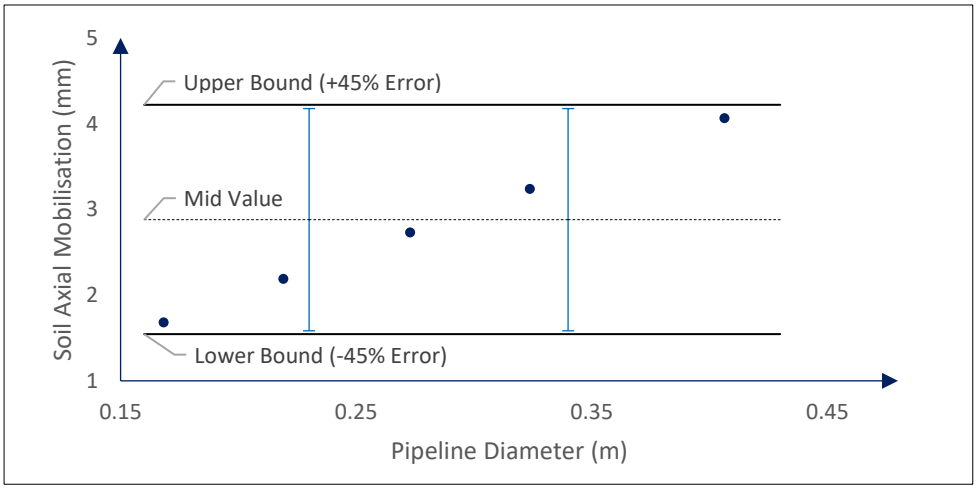

Figure 9. Axial Mobilisation vs Pipeline Diameter

The pipeline diameter, pipeline submerged weight and soil submerged weight are contributing parameters in the soil lateral friction, Eq. (4). For sandy soils, submerged unit weight is density dependent and the densities of loose, medium and dense sands range from 8.5-11.0 N/m^3 , 9.0-12.5 N/m^3 and 10-13.5 N/m^3, respectively [30]. For each pipeline diameter, the values of soil lateral friction

coefficient against soil submerged weight for minimum and maximum pipeline submerged weights can be plotted as shown in Figure 10. The upper and lower groups of the curves represent minimum and maximum pipeline submerged weight, respectively.

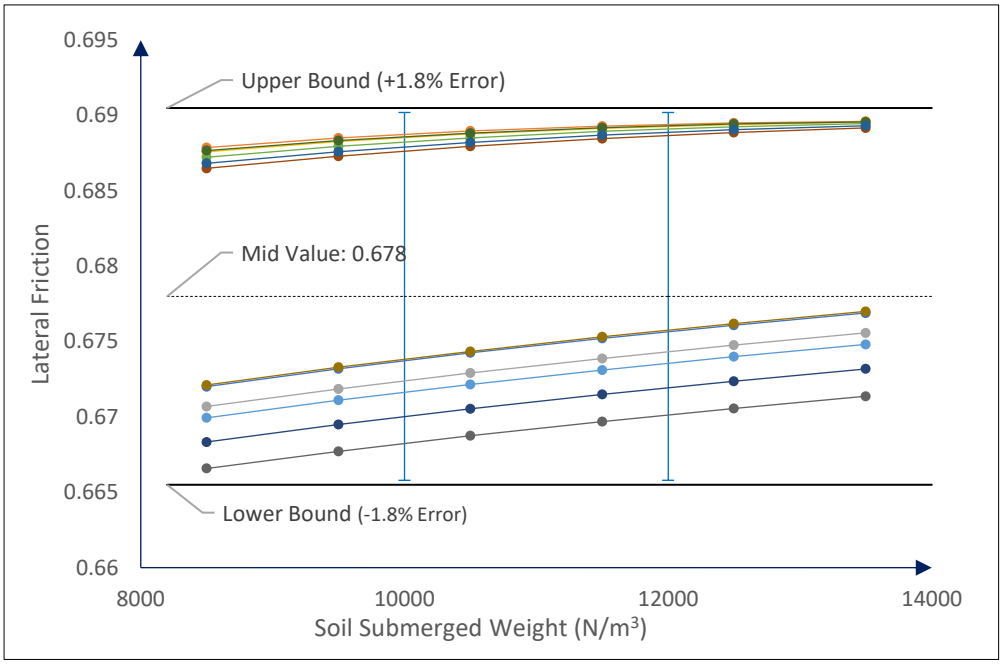

Figure 10. Soil Lateral Friction Coefficient vs Soil Submerged Weight

The 1.8% error bars (vertical lines with end caps) of the best estimate value of the lateral soil friction i.e. 0.678 are also plotted in Figure 10 which clearly show that they can fully encompass the whole range of the values (horizontal solid lines). Considering the wide range of buckling force, a 1.8% error can be treated as negligible and therefore, a fixed value of 0.678 can represent the best estimate of the soil lateral friction. For a specific pipeline by utilising Eq. (9) to Eq. (11) and considering the whole range of soil submerged unit weight stated above, the range of lateral mobilisation can be established.

To construct a pipeline rogue lateral OoS by utilising a single sinusoidal configuration, the values of maximum curvature (κ_{max}) and wavelength (L) are required. There is a limited amount of pipeline as-laid data available in the public domain such as [31]. The most accurate study was carried out by Matheson et al [4] based on a very precise Remotely Operated Vehicle (ROV) survey. They concluded that the pipeline as-laid curvatures can be represented by a normal distribution with mean and standard deviation values of 0 1/m and 0.0002 1/m, respectively. 99.73% of the values lie within +/-3 standard deviations. This suggests that an upper bound of 0.0006 1/m can be assumed for the values of curvature in a deterministic assessment. The lower bound curvature value can be considered 0.0001 1/m as it is practically unlikely to lay a pipeline without such a small curvature (radius of 10 km). For curvature values less than this amount, the CBF approaches infinity which is not of interest. The equivalent sinusoidal wavelength concluded in Matheson's research was 120m.

Based on the analysis undertaken and presented here, contributing parameters in pipeline resistance against lateral buckling (triggered by rogue OoS) together with their ranges are outlined in Table 3. It is to be noted that the ranges stated in this table are valid for the pipelines with a dimeter between 6" to 16" laid on sandy seabeds. The values stated in Table 3 should be used as a starting point (e.g. in a front end engineering study) and field specific values shall be utilised once available.

Parameter	Symbol	Value / Range	Unit
Soil Axial Friction Coefficient	μ_{ax}	0.3 - 1.0	-
Soil Axial Mobilisation	Mob_{ax}	Eq. (3) to Eq. (5)	m
Soil Lateral Friction Coeff.	μ_{lat}	0.678	-
Soil Lateral Mobilisation	Mob_{lat}	Eq. (9) to Eq. (11)	m
As-Laid OoS Wavelength	L	120	m
As-Laid OoS Curvature	κ_{max}	0.0001 - 0.0006	$1/m$

Table 3. Range of Contributing Parameters (Resistance)

An appropriate range of lateral frication coefficient values needs to be established by the user based on the best estimate value stated Table 3. A range from 0.5 to 0.9 seems representative [32] in the absence of project specific information.

7. FRAMEWORK AND NUMERICAL EXAMPLE

A framework is developed and outlined in Figure 11 to calculate the range of critical lateral buckling force at a rogue OoS. This framework utilises the FE modelling technique, rogue lateral OoS construction methodology and identified contributing parameters (and their range) in a structured way.

A numerical example when utilising this framework for a 10" (0.273m) dia, 25.4mm thick pipeline with a weight of 1237 N/m is presented here. The seabed is modelled according to the two-surface contact technique. The pipeline is built by PIPE31 elements and its mesh size is limited to the OD. The PIPE31 is a beam-based element with pipe cross-section which can be subjected to internal and external pressures, and hoop and axial stresses are computed accordingly. At initial stage, the seabed-pipeline tangential (frictional) contact properties are set to zero to provide a friction free contact. This will ensure that the pre-defined shape of the lateral OoS can be applied without any resistance from the soil. The pipeline is placed above the seabed and then lowered onto the seabed by applying the self-weight (W_{sub}) to initiate the normal contacts. Subsequently, pipeline axial, lateral and rotational (in seabed plane) boundary conditions are set to free to provide the pipeline with flexibility to apply the lateral OoS configuration. The OoS profile is constructed based on Eq. 23 by using the values of wavelength and curvature. A python script is developed to calculate the coordinates of the sinusoidal

OoS and to impose it on the straight pipeline as pre-defined displacements. The pipeline-seabed interaction parameters are altered based on Eq. 14 to Eq. 18 and tangential contacts (axial and lateral frictions) are activated. To replicate the fully restrained sections of the pipeline, boundary conditions at the ends are set to fixed (constrained) and temperature is increased gradually. Another python script is used to monitor pipeline effective axial force (EAF) at the crown of the OoS and to specify a point where a sharp drop in EAF is observed. This EAF is considered as the critical buckling force.

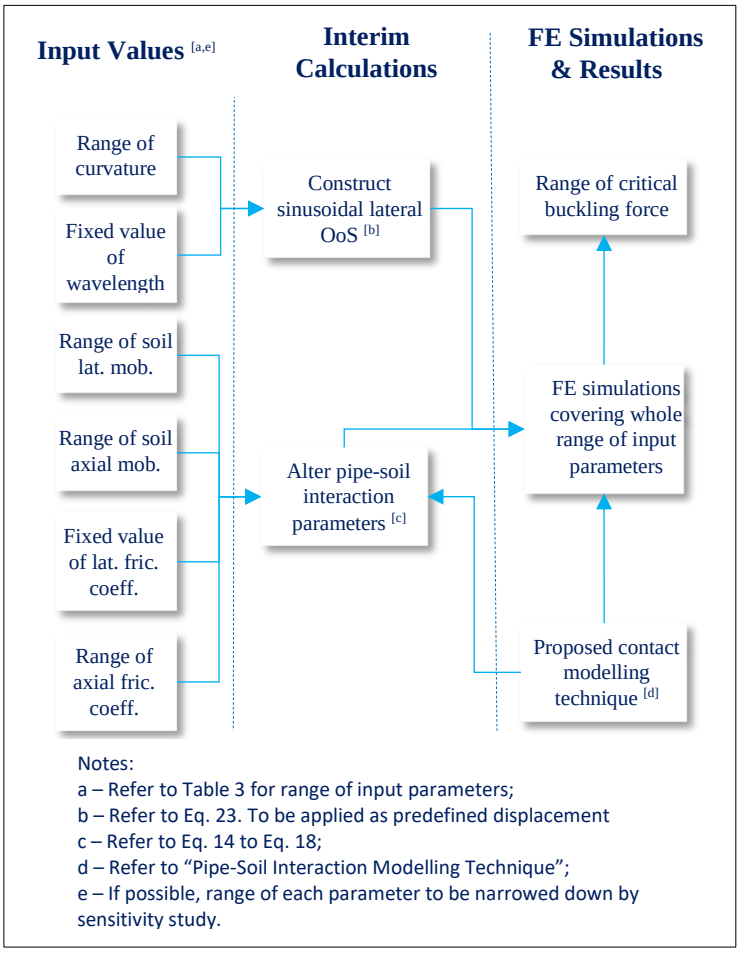

Figure 11. Framework to Compute the Range of Lateral CBF of a Rogue OoS

For all the OoS configurations (combinations of L and κ_{max}), the whole range of pipeline-seabed interaction parameters need to be considered. The ranges of contributing parameters are obtained based on Table 3. Through sensitivity analysis, it was shown that for a specific OoS configuration, effects of axial friction and mobilisation are minimal, and therefore, considered as non-contributing parameters. However, other parameters influence the CBF significantly. The CBF vs soil lateral mobilisation and OoS maximum curvature is plotted in Figure 12 which shows that the range of CBF of the rogue lateral OoS studied in this example can vary from -1360 kN to -7200 kN. In addition, it can be concluded that the value of the soil lateral mobilisation is a key contributor in CBF, specially for lower curvatures. For higher curvature values the CBF remains almost constant and independent of soil lateral mobilisation.

For higher mobilisation values, the variation of CBF against curvature decreases, though. It should be noted that another key contributor is the lateral friction which was not studied here as the intention of this example was to show the impact of other parameters. However, the same approach can be utilised to obtain a wider range of the CBF by varying the lateral friction.

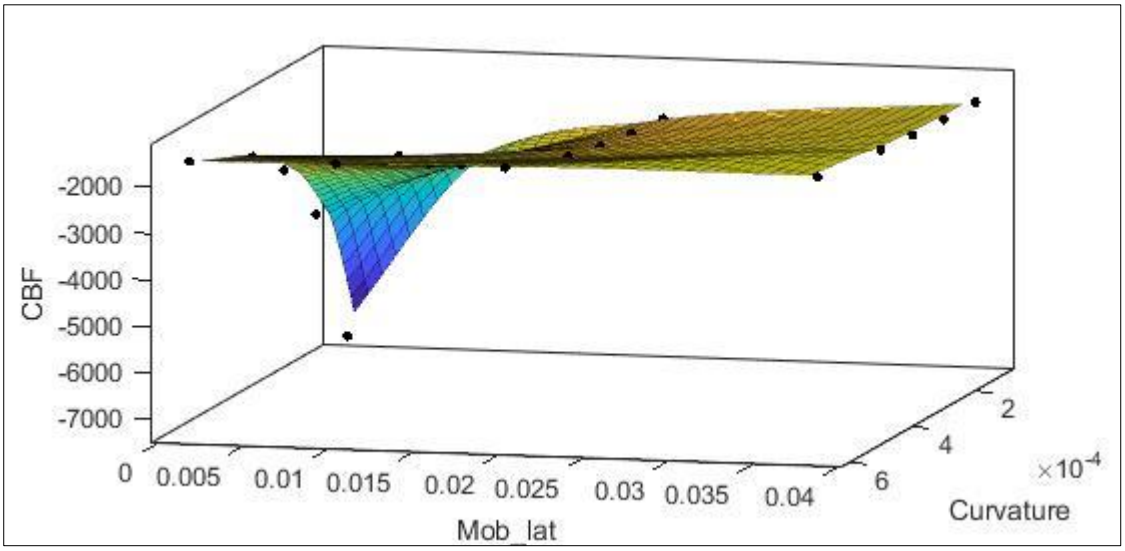

Figure 12. CBF vs Soil Lateral Mobilisation and OoS Curvature

The results can be fed into the design of the buckle initiators (e.g. sleepers). Figure 13 presents a screenshot of an Abaqus FE model where the sleeper height is selected so that the CBF at the sleeper is smaller than the whole range of the CBF of rogue lateral OoS (-1360 kN to -7200 kN). This resulted in formation of the desired buckles at the locations of the sleepers only.

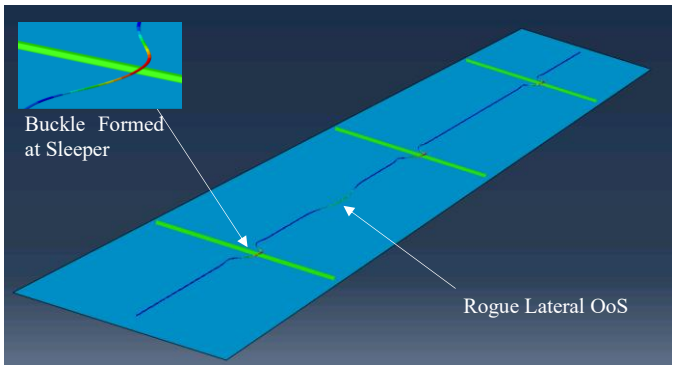

Figure 13. Abaqus Screenshot - Deliberate Buck Formation at Sleepers

Figure 14 shows the same pipeline but with sleepers shorter in height leading to the CBF at sleepers being greater than the CBF at the adjacent rogue lateral OoS and therefore, an unwanted lateral buckle is formed.

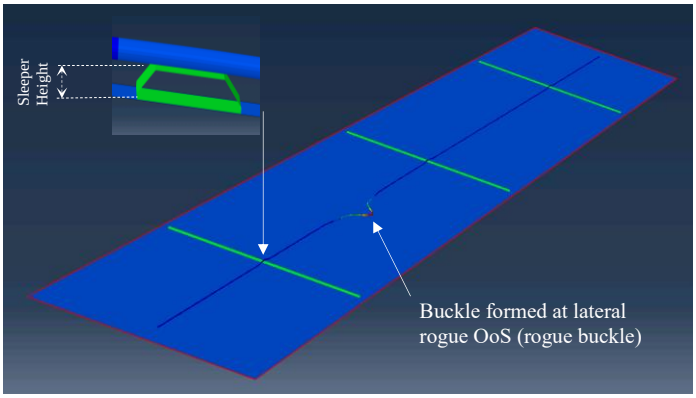

Figure 14. Tangential Unwanted buckle formation at rogue lateral OoS

The shape of the rogue buckle on the seabed is influenced by the shape and orientation of the initial OoS which is in the form of a symmetric sinusoidal deflection in this example, representing the first mode of buckling. The initial OoS was superimposed so that it was aligned with the pipeline direction. As a result of this, the rogue buckle is initiated and developed symmetrically and perpendicularly to the pipeline direction. However, the modelling technique can adopt unsymmetrical buckling. By defining and imposing any desired initial OoS such as unsymmetrical and angled or shapes representing other modes of buckling in the FE model, buckles can be developed unsymmetrically and angled to the pipeline direction.

It is worth mentioning that the field observations including comparison between pipeline as-laid OoS against the buckles which were initiated post start-up have demonstrated that FE simulation can successfully be deployed to predict the buckle initiation and formation at the rogue lateral OoS location as well as sleepers [4]. In addition, experiments based on physical models have shown that the buckle initiation triggers at sleepers [35].

8. CONCLUSIONS

The work outlined in this paper introduced a simplified pipeline-seabed interaction constitutive relationship for sandy seabeds to study the initiation of the buckles at rogue lateral OoS locations. The proposed FE modelling technique benefits from a two-surface seabed which can correctly capture and decouple axial and lateral pipe-soil interaction behaviour as required by the constitutive relationships. This technique eliminates the need for user-defined friction subroutines in Abaqus FE software which is a technically complex task. Various methods of constructing a rogue lateral OoS were studied and it was concluded that a single sinusoidal curve, characterised by its wavelength and curvature is the most suitable approach. The contributing parameters and relevant dependencies in CBF were developed and it was shown that the full range of contributing parameters outlined in Table 3 need to be considered. This study provides a framework and a numerical example to compute the range of CBF of a rogue lateral OoS. The numerical example demonstrated (a) the significant impact of the soil lateral

mobilisation and OoS curvature on the CBF especially at lower curvatures, (b) decrease in the variation of CBF (against curvature) for higher mobilisation values and (c) independency of the CBF against soil axial friction and mobilisation. In addition, it was shown that the outcome of the study can be fed into the design of the buckle initiators (e.g. sleepers) to ensure buckles are formed at the engineered locations rather than the seabed.

This work enables parametric studies to further narrow down the range / number of contributing parameters and to establish the critical lateral buckling response surfaces. Such surfaces can be used to undertake deterministic and probabilistic assessments to establish the reliability of the buckle initiation at the engineered buckling locations.

REFERENCES

1 Bai, Q., Qi, X., Brunner, M., 2009. Global Buckle Control with Dual Sleepers in HPHT Pipelines. Offshore Technology Conference, OTC 19888.

2 Sun, J., Jukes, P., Shi, P., 2012. Thermal Expansion / Global Buckling Mitigation on HPHT Deepwater Pipelines, Sleepers or Buoyancy?. Proceedings of the Twenty-Second International Offshore and Polar Engineering Conference.

3 Harrison, G.E., Brunner, M.S., Bruton, D.A.S., 2003. King Flow lines – Thermal Expansion Design and Implementation. Offshore Technology Conference, OTC 15310.

4 Matheson, I., Carr, M., Peek, R., Saunders, P., Georg, N., 2004. Penguins Flowline Lateral Buckling Formation Analysis and Verification. Proceedings of the 23rd International Conference on Offshore Mechanics and Arctic Engineering (OMAE).

5 Hobbs, R.E., 1984. In-Service Buckling of Heated Pipelines. Journal of Transportation Engineering, 110(2), 175-189.

6 Hobbs, R.E., Liang, F., 1989. Thermal Buckling of Pipelines Close to Restrains. International Conference of Offshore Mechanics and Arctic Engineering.

7 Taylor, N., Gan, A.B., 1986. Submarine Pipeline Buckling - Imperfection Studies. Thin-Walled Structures 4, 295-323.

8 Maltby, T.C., Calladine, C.R., 1995. An Investigation into Upheaval Buckling of Buried Pipelines – II Theory and Analysis of Experimental Observations. Int. J. Mech. Sci., Vo. 37.

9 Karampour, H., Albermani, F., Gross, J., 2013. On Lateral and Upheaval buckling of Subsea Pipelines. Engineering Structures 52.

10 Abaqus 6.19, 2019. Analysis User's Guide. Volume V, Prescribed Conditions, Constraints & Interactions.

11 Abaqus 6.19, 2019. Theory Guide. Surface Interactions, Coulomb Friction.

12 Yang, F., Tian, Y., 2014. Development of ABAQUS User Subroutine for Advanced Pipe/Soil Modelling. CEED Seminar Proceedings.

13 Hong, Z., Liu, R., 2018. Submarine Pipeline Lateral Global Buckling and Buckling Failure Critical State Discussion. Journal of Harbin Institute of Technology.

14 Stutz, H., Masin, D., Sattari, A.S., Wuttke, F., 2017. A General Approach to Model Interfaces using Existing Soil Constitutive Models Application to Hypoplasticity. Computer and Geotechnics 87, 115-127.

15 Rathbone, A., Cumming, G., 2010. A Holistic Design Approach for Considering Rogue Buckle Formation due to Pipelay-Induced Out-of-Straightness. Proceedings of the ASME 2010 29th International Conference on Ocean, Offshore and Arctic Engineering (OMAE).

16 Rathbone, A.D., Tornes, K., Cumming, G., Roberts, C., 2008. Effect of Lateral Pipelay Imperfection on Global Buckling Design. Proceedings of the Eighteenth International Offshore and Polar Engineering Conference.

17 White, D., Cheuk, C.Y., 2008. Modelling the Soil Resistance on Seabed Pipelines during Large Cycles of Lateral Displacement. Marine Structures 21, 59-79.

18 White, D.J., Cathie, D.N., 2011. Geotechnics for subsea pipelines. Proc. 2nd Int. Symp. on Frontiers in Offshore Geotechnics (ISFOG), 87-123.

19 White, D.J., Westgate, Z.J., Ballard, J.C., De Brier, C., Bransby, F., 2015. Best Practice Geotechnical Characterisation and Pipe-soil Interaction Analysis for HPHT Pipeline Design. Proc. Offshore Technology Conference OTC 26026.

20 Palmer, A.C., Steenfelt, J.S., Steensen-Bach, J.O., Jacobsen, V., 1988. Lateral Resistance of Marine Pipelines on Sand. Offshore Technology Conference, OTC 5853.

21 Verley, R.L.P., Sotberg, T., 1992. A Soil Resistance Model for Pipelines Placed on Sandy Soils. Proc. Of the Conference on Offshore, Marine and Arctic Engineering, OMAE, Volume 5, 123-131.

22 DNVGL-RP-F114, 2017. Recommended Practice - Pipe-Soil Interaction for Submarine Pipelines.

23 Wang, D., White, D.J., Randolph, M.F., 2010. Large-Deformation Finite Element Analysis of Pipe Penetration and Large Amplitude Lateral Displacement. Canadian Geotechnical Journal.

24 Chatterjee, S., White, D., Randolph, M., 2012. Simulations of Pipe–Soil Interaction during Large Lateral Movements on Clay. Géotechnique.

25 White, D.J., Randolph, M.F., 2007. Seabed Characterisation and Models for Pipeline-Soil Interaction. International Journal of Offshore and Polar Engineering, 17(3), 193-204.

26 Bruton, D., White, D., Cheuk, C., Bolton, M., Carr, M., 2009. Pipe/Soil Interaction Behaviour During Lateral Buckling, Including Large-Amplitude Cyclic Displacement Test by the Safebuck JIP. Offshore Technology Conference, OTC 17944.

27 DNVGL-ST-F101, 2017. Standard - Submarine Pipeline Systems.

28 Vosooghi, N., Ivanovic, A., Sriramula, S., 2016. Contribution of Axial Soil Resistance in Buckle Initiation of the HPHT Pipelines on Sleepers. Proceedings of the ASME Conference on Ocean, Offshore and Arctic Engineering, OMAE2016-54137.

29 ASME B36.10M, 2018. Welded and Seamless Wrought Steel Pipe.

30 DNV-RP-F105, 2006. Recommended Practice - Free Spanning Pipelines.

31 Brown, G., Brunner, M., Qi, X., 2006. Lateral Buckling Reliability Calculation Methodology Accounting for Buckle Interaction. Offshore Technology Conference, OTC 17795.

32 PD 8010-2, 2004. Code of Practice for Pipelines – Part 2: Subsea Pipelines.

33 Abaqus 6.19, 2019. Analysis User's Guide. Volume I, Analytical Rigid Surface Definition.

34 DNVGL-RP-F110, 2018. Recommended Practice - Global Buckling of Submarine Pipelines.

35 Silva-Junior, H.C., Cardoso, C.O., Carmigtotto, M.A.P., Zanutto, J.C., 2008. Reduced Model Device of Solutions to Control Thermal Buckling Effects in HP-HT Subsea Pipelines. 27th International Conference on Offshore Mechanics and Arctic Engineering, OMAE 57637.

36 Fredsoe, J., 2016. Pipeline-Seabed Interaction. Journal of Waterway, Port, Coastal, and Ocean Engineering.

37 Suresh Kumar, D., Achani, D., Sunny, M.R., Sahoo, T., 2019. Influence of Wave-Induced Uplift Forces on Upheaval Buckling of Pipelines Buried in Sandy Seabeds. Journal of Offshore Mechanics and Arctic Engineering.